Calibration of the CLF Andor iKon Indirect Detection X-ray Camera

Contact: jonathan.wood08@imperial.ac.uk

J. C. Wood, S. P. D. Mangles, Z. Najmudin
The John Adams Institute for Accelerator Science, Blackett Laboratory, Imperial College London, United Kingdom.

R. J. Clarke, D. R. Symes
Central Laser Facility, STFC Rutherford Appleton Laboratory, Chilton, United Kingdom.

Abstract

A calibration was performed to facilitate the conversion of camera counts to x-ray energy deposited in the scintillator for the CLF's Andor iKon L 936 camera, which is a scientific CCD camera fibre-coupled to a structured 150 μm thick caesium iodide scintillator. To perform this calibration the camera was exposed to a disk source of iron-55 with a known activity emitting a known spectrum of x-rays. It was shown that it is improper to model this source as a point source, and a model was described to account for this source geometry. By comparing the model of the source to the data, it was found that this camera produces (0.245 ± 0.002) counts per keV of energy deposited into the scintillator with $1\times$ gain.

1 Introduction

There are numerous methods of producing x-rays via high intensity laser interactions with matter. Examples include high harmonic generation [1], betatron radiation from laser wakefield accelerators [2] or bremsstrahlung from hot electrons moving through a solid density target [3]. When investigating the properties of an x-ray source, it is desirable to measure the total energy it emits. If a spectral shape can be assumed or measured, the total energy can then be converted in to a number of photons. One method of measuring the emitted energy is to expose a calibrated x-ray camera, which takes up some known solid angle, to the source.

To detect hard x-rays (> 10 keV), imaging systems based on indirect detection are common. In this scheme x-ray photons are absorbed by a scintillator, and the visible light produced is imaged on to a camera. For hard x-ray detection, the CLF owns an Andor iKon L 936 indirect detection camera [4]. The system consists of a 150 μm thick structured caesium iodide (CsI) scintillator doped with thallium (a Hamamatsu J6677-01 [5]) held against a fibre bundle which is coupled to the camera's CCD. Scintillators emit a number of visible photons that is directly proportional to the energy deposited in them. The constant of proportionality is known for many scintillation materials but what is not known for this device is how many of these scintillation photons are detected by the CCD. Some will be lost because they do not travel towards the CCD, others will be lost in the optical fibre bundles and more because of the quantum efficiency of the CCD. Furthermore, what is read out in the image is some number of counts that is proportional to the number of detected scintillation photons. As a result it is necessary to calibrate the camera with a well characterised source so that the number of counts on an image can be converted to x-ray energy deposited in the CsI scintillator. This work has allowed for a calculation of the number of photons emitted from a betatron radiation source driven by the Gemini laser [6].

2 Calibration Method

The number of photons in an x-ray beam incident on a camera between energies E_{min} and E_{max} is related to the number of camera counts C by the equation

$$C = \alpha N_p \int_{E_{min}}^{E_{max}} E\ S(E)\ T(E)\ Q(E)\ dE \qquad (1)$$

where α is the x-ray counts per keV deposited in the scintillator. All energies E in this equation are measured in keV. The spectrum S has been normalised such that $\int_{E_{min}}^{E_{max}} S(E)dE = 1$. T is the transmission of any materials between the source and the detector and Q is the quantum efficiency of the scintillator. Assuming that $T(E)$ and $Q(E)$ are known, to perform a calibration, i.e. to determine α from C, a source irradiating the scintillator with a known number of photons N_p, with a known spectrum $S(E)$, is required. Therefore radioactive sources are a popular choice for calibrations. Once α is known the number of photons can be calculated from C if the spectral shape is known.

The camera was calibrated using a radioactive iron-55 source of activity $A_{Fe} = (23.6 \pm 0.1)$ MBq. Its half life is 2.737 years, so the activity of the source can be assumed constant over the experiment. It emits moderate energy x-rays mostly at 5.9 keV, which are energetic enough to produce a reasonable response in the scintillator. From [7, 8] one can calculate that one moderate energy x-ray is emitted in 27.25% of iron-55 decays with the energies E_i and probabilities p_i given in table 1. The rest of the decays happen via an Auger process where no x-ray is emitted. X-rays at 0.64 keV are also emitted, but they have been igonred as they would have been absorbed before reaching the scintillator, and they are emitted relatively infrequently. This is why $\sum_i p_i$ is slightly less than 1. The source activity implies that $(6.49 \pm 0.03) \times 10^6$

Photon Energy E_i/keV	Relative Probability p_i
5.888	0.30
5.899	0.59
6.49	0.104

Table 1: Photon emission from Fe-55 decay [8]. X-rays at 0.64 keV, which are emitted infrequently and are absorbed before reaching the scintillator, have been omitted from the table.

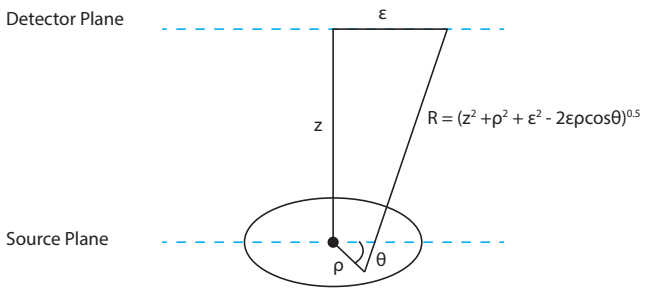

Figure 1: Geometry of the disk source problem.

x-rays are emitted per second in to 4π steradians. We will return to the issue of geometry shortly. The average energy absorbed in the scintillator per incident x-ray photon $\langle E_{dep} \rangle$ is calculated using the equation

$$\langle E_{dep} \rangle = \frac{\sum_i E_i \; p_i \; T(E_i) \; Q(E_i)}{\sum_i p_i} \tag{2}$$

where is the quantum efficiency Q was assumed to be equal to the absorption fraction of photons of energy E_i in 150 μm thick CsI. $T(E_i)$ is the fractional transmission of photons of energy E_i through all materials between the source and the scintillator, including the air and the 40 μm inorganic parylene layer that protects the scintillator [9]. Q is present in the expression because not every photon will be absorbed in the scintillator, which reduces the average deposited energy per photon incident on the scintillator. For this camera $\langle E_{dep} \rangle = 5.56\,\text{keV}$. Now that the total source activity and the average energy absorbed per photon incident on the scintillator are known, the fraction of emitted photons that travel in to the solid angle taken up by the scintillator must be calculated. Once this is known the total energy delivered to the scintillator can be calculated.

The source was a (12.5 ± 0.1) mm diameter disk in a holder with an (11.0 ± 0.1) mm circular aperture, where the errors are the specified engineering tolerances. This was placed close to the scintillator at the front of the camera. It was difficult to measure this distance accurately because of radiological safety issues, however it is possible to calculate it from the shape of the detected intensity pattern. Near to an extended source the source does not act as a point source. For a circular disk, the fall off in radiation dose with distance is instead described in [10]. The geometry used in the calculation is shown in figure 1. The dose D delivered to a point of distance ϵ from the centre of the detector is described by the equation

$$D(z, \epsilon) = \int_0^a \int_0^{2\pi} G(R) \; S(\rho) \; \rho \; d\rho \; d\theta \tag{3}$$

where ρ and θ are the radial and azimuthal coordinates on the disk source respectively, and z is the shortest distance from the plane of the disk to the plane of the detector. a is the source radius. From figure 1 the distance from some point (r, θ) on the source to position ϵ on the detector is $R = [z^2 + \rho^2 + \epsilon^2 - 2\epsilon\rho\cos\theta]^{\frac{1}{2}}$. $S(\rho)$ is the source strength per unit area which is assumed to be constant here. The detector response $G(R) = \cos\psi/(4\pi R^2)$, where ψ is the angle between the detector surface and R; therefore $\cos\psi = z/R$. This term arises as a consequence of the source being close to the detector: rays from the source subtend a significant angle ψ to the detector. For a small detector far from the source $\cos\psi \to 1$. The integration over the surface of the source in equation 3 simply accounts for the form factor of the extended source.

The validity of equation 3 can be checked by testing what happens in the limit of small and large displacement z from the source. Far from the source ($z \gg a$) the source should look like a point source. To simplify the workings, we observe the source with a small detector placed on-axis such that $\epsilon = 0$. For large z, $R \approx z$ and $cos\psi = z/R \approx 1$, so the equation simplifies to

$$D(R, 0) = \frac{1}{4\pi R^2} S_0 \pi a^2 \tag{4}$$

where $S_0\pi a^2$ is the total activity of the source (assuming a constant source activity) and z has been explicitly replaced by R. This is what would be expected from a point source. It can be shown [11] that as $z \to 0$ equation 3 tends towards $D = \frac{1}{2}S(\rho)$, as expected from elementary considerations.

Example intensity patterns calculated using this equation for an 11 mm circular source and 27.6 mm side length detector, the same as the camera being calibrated, are shown in figure 2 for $z = 5$ mm and $z = 15$ mm. These images demonstrate that the intensity pattern is not isotropic and does not follow an inverse square law: as the distance from the source triples the peak intensity falls by a factor of ~ 5, not 9. As the calculation was computationally expensive, requiring a double integration for each detector pixel, it was performed for a reduced 200×200 pixel detector rather than the 2048×2048 pixels of the real detector.

3 Results

The Andor indirect detection camera was exposed to the iron-55 source for nine 60 second long measurements.

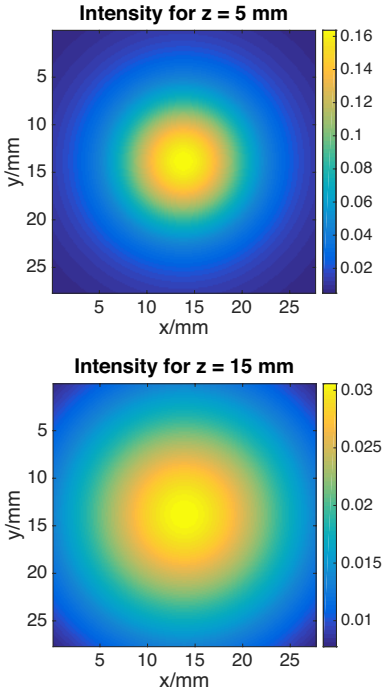

Figure 2: Intensity patterns produced by an 11 mm diameter circular source at distances $z = 5$ mm and $z = 15$ mm from the source, for a detector of side length 27.6 mm.

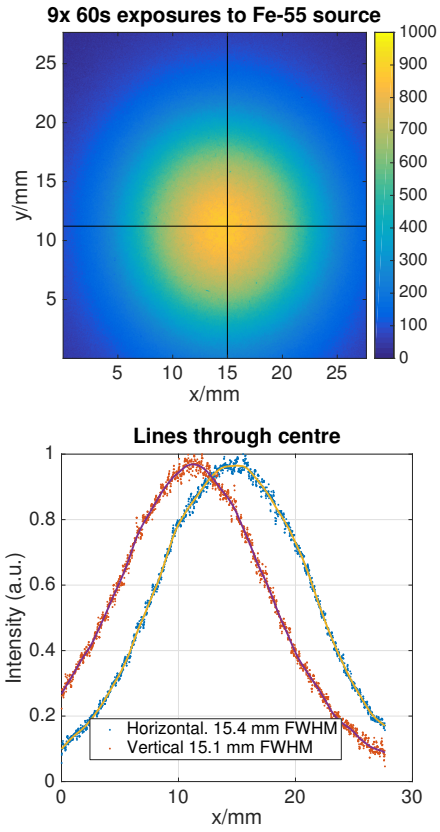

Figure 3: Top: sum of nine 60 second camera exposures to the iron-55 source. The black lines go through the centre of the intensity pattern. The lineouts shown at the bottom were taken along these lines.

The camera chip was cooled to $-15\,^{\circ}$C, a gain setting of $1\times$ was applied with a readout rate of 1 MHz, and 16-bit images were recorded. Note that this calibration is valid for other chip temperatures and readout rates, but not different gain settings. Over 60 seconds a significant amount of dark noise accumulated on the chip, in addition to the read noise introduced by the readout electronics, which must be corrected for. To do so a series of ten 60 second exposures were taken without the source. Out of ten, three images had no hot pixels caused by cosmic ray interactions, and these were averaged to produce a mean background image of the camera noise which was subtracted from each of the nine data images. It is better to do this correction pixel by pixel, a process called dark field correction, than subtracting a mean number of counts from all pixels because each chip has a unique pattern of dark noise [12]. The difference between any single dark field image and the mean dark field image was an average of ~ 0.11 counts/pixel. Therefore the error on nine dark field subtractions was 0.035 counts/pixel, or 1.5×10^5 counts summed over the whole image.

The sum of the nine dark field corrected 60 second exposures is shown at the top of figure 3, where the black lines cross at the peak of the intensity pattern. Lineouts along these lines, shown at the bottom of the figure, were fitted with a cubic smoothing spline, revealing that the intensity pattern had FWHM widths of 15.4 mm and 15.1 mm in the horizontal and vertical directions respectively. The difference is attributed to a slight misalignment of the source with respect to the detector. The average of these values was taken as the real width at (15.25 ± 0.10) mm, where the error is the resolution of the scintillator. This width was compared to the calculated FWHM widths from a range of trial source detector separations (z) going from 1 mm to 20 mm in 1 mm steps. Minimising the difference between the measured and estimated widths revealed a best fit $z_0 = (7.56 \pm 0.11)$ mm. The sub-mm resolution was possible by interpolating the widths of the trial patterns on to a finer spatial scale, and the error was propagated from the uncertainty in the measured FWHM of the intensity distribution. This is within the range of expected values from the measured geometry of the source holder and camera.

The apparent source strength S_0 for this source is given by

$$S_0 = \frac{0.2725\ A_{Fe}\,\langle E_{dep}\rangle\,\tau_{aq}}{\pi a^2} \tag{5}$$

where $0.2725 A_{Fe}$ is the number of x-ray photons emitted per second and τ_{aq} is the acquisition time. Note that the quantum efficiency of the camera and material transmission is contained in this equation via the $\langle E_{dep}\rangle$

term, therefore this is a modified source strength to account for photons that can be detected by the camera. Assuming that this does not vary spatially across the source equation 3 can be re-written as

$$D(z, \epsilon_x, \epsilon_y) = S_0 \int_0^a \int_0^{2\pi} G(R)\ \rho\ d\rho\ d\theta \qquad (6)$$

where ϵ_x and ϵ_y are the cartesian coordinate system on the detector. Since z, a and S_0 are known, D can now be calculated for each detector pixel, and the total energy deposited in the scintillator E_s is given by

$$E_s = \int_{\epsilon_{x,min}}^{\epsilon_{x,max}} \int_{\epsilon_{y,min}}^{\epsilon_{y,max}} D(z_0, \epsilon_x, \epsilon_y)\ d\epsilon_x\ d\epsilon_y \qquad (7)$$

Evaluating this integral revealed that over the nine exposures a total energy of $(5.16 \pm 0.05) \times 10^9$ keV was absorbed by the scintillator. The error was calculated by propagating, separately, the errors in the disk source size and the distance from the source to the detector and then summing the fractional errors in quadrature with the error in the source activity. The Poisson error due to the random nature of radioactive decay was ignored because it was of order 10^{-5}. A total of $(1.2673 \pm 0.0002) \times 10^9$ camera counts were recorded, where the error comes from the dark field subtraction. Therefore the camera records (0.245 ± 0.002) counts/keV of energy deposited.

This method would be suitable for characterising any direct or indirect detection x-ray camera, along with other forms of x-ray detector such as Fujifilm image plate. For harder x-ray detectors the method will remain valid but a harder source of x-rays may be necessary, such as an americium-241 source.

This method was also applied to a Princeton Instruments PIXIS-XF camera [13], which had the same model of CsI scintillator fibre coupled to a CCD, although the scintillator was held behind a 250 μm thick beryllium window. The counts/keV conversion factor as a function of gain setting is shown in table 2, where data was taken in single 300 second long exposures. The

Gain	Counts/keV
Low	0.056 ± 0.001
Medium	0.106 ± 0.002
High	0.84 ± 0.01

Table 2: Number of camera counts per keV of energy deposited in to a 150 μm thick CsI scintillator in front of a Princeton Instruments PIXIS-XF camera.

table shows that the Andor camera is more than 4 times more sensitive at the lowest gain setting, making this a much better choice for high signal to noise ratio imaging.

4 Conclusion

This report detailed the calibration of the CLF's Andor iKon L 936 camera, which is a scientific CCD camera fibre-coupled to a structured 150 μm thick CsI scintillator. The purpose of the calibration was to provide a conversion factor between the number of camera counts and the x-ray energy deposited in to the scintillator. This was achieved by exposing the scintillator to an iron-55 source that emitted a known spectrum of x-rays with a known activity. It was shown that it is important to pay careful consideration to the source-detector geometry because the source could not be described by a point source. It was found that a deposition of 1 keV of x-ray energy in to the scintillator resulted in (0.245 ± 0.002) counts being produced on the camera.

5 Acknowledgements

We acknowledge funding from STFC for the support of the John Adams Institute of Accelerator Science by grants ST/J002062/1 and ST/P000835/1.

References

[1] R. A. Ganeev *High-order harmonic generation in a laser plasma: a review of recent achievements*. J. Phys. B: At. Mol. Opt. Phys. 40 R213R253, 2007.

[2] S. Corde et al. *Femtosecond x rays from laser-plasma accelerators*. Reviews of Modern Physics 85(1), January-March 2013.

[3] D. Giulietti et al. *X-ray emission from laser-produced plasmas*. L.A. Riv. Nuovo Cim. 21(1), 1998.

[4] Andor Technology, *Andor iKon-L Series*, Datasheet, Available at `http://www.andor.com/pdfs/specifications/Andor_iKon-L_936_Specifications.pdf`. 14/06/2016.

[5] Hamamatsu, *X-ray Scintillator*, Datasheet. Available at `http://www.andor.com/pdfs/specifications/Andor_High_Energy_iKonM_SO.pdf`. 14/06/2016.

[6] J. C. Wood et al., *Enhanced Betatron Radiation from a Laser Wakefield Accelerator in a Long Focal Length Geometry*. In preparation. 2017.

[7] AEA Technology, *Sources datasheet*. 2011.

[8] Brookhaven National Laboratory, *NuDat 2.6 Database*. `http://www.nndc.bnl.gov/nudat2/`. Accessed 23/06/2016.

[9] S. Whitbread, Hamamatsu Photonics UK Limited. *Private communication*. 2016.

[10] J. Smith et al. *Generalized Off-Axis Distributions from Disk Sources of Radiation*. J. Appl. Phys. 1954, pp. 519-527.

[11] J. T. Conway. *Calculations for a disk source and a general detector using a radiation vector potential*. Nucl. Instruments Methods Phys. Res. Sect A Accel. Spectrometers, Detect. Assoc. Equip. 589(1), 2008, pp. 20-33.

[12] Princeton Instruments. *PIXIS-XF System User Manual*. 2011.

[13] Princeton Instruments X-ray Group. *PIXIS-XF: 2048*. Datasheet. Available at `http://www.princetoninstruments.com/userfiles/files/assetLibrary/Datasheets/Princeton-Instruments-PIXIS_XF_2048B_rev_N1_1-10-14-15.pdf`. Accessed 14/06/2016.